Composite Structures 93 (2011) 831–842

Contents lists available at ScienceDirect

Composite Structures

journal homepage: www.elsevier.com/locate/compstruct

A further discussion of nonlinear mechanical behavior for FGM beams under in-plane thermal loading

L.S. Ma [a,b], D.W. Lee [b,*]

[a] School of Science, Lanzhou University of Technology, Lanzhou 730050, China
[b] MEMS & Nanotechnology Laboratory, School of Mechanical Systems Engineering, Chonnam National University, Gwangju 500-757, Republic of Korea

ARTICLE INFO

Article history:
Available online 10 August 2010

Keywords:
Functionally graded material beam
Static behavior
Dynamic response
In-plane loading
Temperature-dependent material properties
Transverse shear deformation

ABSTRACT

Due to the variation in material properties through the thickness, bifurcation buckling cannot generally occur for plates or beams made of functionally graded materials (FGM) with simply supported edges. Further investigation in this paper indicates that FGM beams subjected to an in-plane thermal loading do exhibit some unique and interesting characteristics in both static and dynamic behaviors, particularly when effects of transverse shear deformation and the temperature-dependent material properties are simultaneously taken into account. In the analysis, based on the nonlinear first-order shear deformation beam theory (FBT) and the physical neutral surface concept, governing equations for both the static behavior and the dynamic response of FGM beams subjected to uniform in-plane thermal loading are derived. Then, a shooting method is employed to numerically solve the resulting equations. The material properties of the beams are assumed to be graded in the thickness direction according to a simple power law distribution in terms of the volume fractions of the constituents, and to be temperature-dependent. The effects of material constants, transverse shear deformation, temperature-dependent material properties, in-plane loading and boundary conditions on the nonlinear behavior of FGM beams are discussed in detail.

1. Introduction

This paper is concerned with the mechanical behaviors of beams made of functionally graded materials (FGM) under an in-plane loading. The extremely complicated bending caused by in-plane thermal loading for beams with simply supported ends is included in the analysis. It is found that the response of load–frequency for the beams is quite different from what was observed in the analysis for beams made of pure materials when effects of both the transverse shear deformation and the temperature-dependent material properties are simultaneously taken into account.

Many studies have been conducted on the static and dynamic behavior of FGM beams. Librescu et al. [1] studied the behavior of thin-walled beams made of FGM operating at high temperatures, which included vibration and instability analysis along with the effects of volume fraction and temperature gradients. A review of various investigations on FGM including thermo-mechanical studies is found in Birman and Byrd [2]. Employing the finite element method, Bhangale and Ganesan [3] carried out thermo-elastic buckling and vibration analysis of a sandwich beam made of FGM. Based on the two-dimensional theory of elasticity, Ying et al. [4] presented solutions for bending and free vibration of FGM beams resting on a Winkler–Pasternak elastic foundation. Static, free and wave propagation analyses were carried out by Chakraborty et al. [5] to examine the behavioral difference in FGM beams. Aydogdu and Taskin [6] investigated the free vibration behavior of a simply supported FGM beam by using classical beam theory, parabolic shear deformation theory and exponential shear deformation theory. Kapuria et al. [7] presented a finite element model for static and free vibration responses of layered FGM beams using an efficient third order zigzag theory for estimating the effective modulus of elasticity and its experimental validation for two different FGM systems under various boundary conditions. Yang and Chen [8] studied the free vibration and elastic buckling of FGM beams with open edge cracks by using classical beam theory. Li [9] proposed a new unified approach to investigate the static and the free vibration behavior of Euler–Bernoulli and Timoshenko beams. Using the modal expansion technique, Yang et al. [10] investigated both free and forced vibrations of cracked FGM beams subjected to an axial force and a moving load. Xiang and Yang [11] studied both free and forced vibrations of an FGM beam with variable thickness under thermally induced initial stresses based on the Timoshenko beam theory. The free vibration of orthotropic FGM beams under various end support conditions was investigated by Lu and Chen [12]. They used an approximate laminate model and a hybrid state-space differential quadrature method to find the semi-analytical solutions based on the two-dimensional theory of elastic-

* Corresponding author. Tel.: +82 62 530 1684; fax: +82 62 530 1689.
E-mail address: mems@chonnam.ac.kr (D.W. Lee).

0263-8223/$ - see front matter © 2010 Elsevier Ltd. All rights reserved.
doi:10.1016/j.compstruct.2010.07.011

ity. Zhong and Yu [13] presented a general two-dimensional solution for a cantilever beam in terms of Airy's stress function. Recently, a new beam theory was presented by Sina et al. [14] to analyze free vibration of FGM beams. Using the modified differential quadrature method, Pradhan and Murmu [15] carried out thermo-mechanical vibration analysis of FGM beams and sandwich beams resting on a variable Winkler foundation. The free vibration characteristics and the dynamic behavior of a simply supported FGM beam under a concentrated moving harmonic load were investigated by Simsek and Kocatürk [16]. Li and Shi [17] proposed a state-space method based differential quadrature to study the free vibration of a functionally graded piezoelectric material beam under different boundary conditions.

Variation in material properties through the thickness of FGM plates or beams results in quite different behaviors for plates or beams made of pure materials under both static and dynamic loading conditions. For example, bifurcation buckling generally cannot occur for FGM plates or beams with simply supported edges due to in-plane loading. Transverse deflection is initiated, regardless of the magnitude of the loading, as is often the case with laminated composite materials [18–20]. The phenomenon was taken into account by Shen [21] and Aydogdu [22]. Shen [21] stated that bifurcation buckling does not take place for FGM rectangular plates with simply supported edges due to the bending–stretching coupling. In the past, several analyses had been reported concerning the buckling of FGM plates, which cannot exist physically, as pointed out by Qatu and Leissa [20]. The flatness conditions of an FGM plate during the pre-buckling stage were presented by Aydogdu [22]. However, few researchers have further studied these special behaviors of FGM plates or beams in detail. Shen [23] analyzed the influence of various factors such as thermal loading and in-plane boundary conditions on the nonlinear bending of FGM plates. nonlinear bending and post-buckling of an FGM circular plate under a thermal loading and uniform radial pressure, respectively, were investigated by Ma and Wang [24,25]. They found that transverse deflections occur immediately when an in-plane compressive load is applied to a simply supported FGM circular plate.

To the authors' knowledge, no researchers have given much attention to the static behavior of FGM beams with simply supported edges due to an in-plane loading. The vibrational response of buckled or bended FGM beams due to an in-plane loading has not been studied when transverse shear deformation in conjunction with temperature-dependent material properties are taken into consideration. These are the primary objectives of the present investigation.

Stretching–bending coupling does not exist in the constitutive equations for an FGM plate when the coordinate system is located at the physical neutral surface of the plate [26,27], therefore, the governing equations and boundary conditions for the FGM plate can be simplified. In the present investigation, based on the nonlinear first-order shear deformation beam theory (FBT) and the physical neutral surface concept, governing equations for both the static behavior and dynamic response of FGM beams subjected to a uniform in-plane thermal loading are derived; then, a shooting method is employed to numerically solve the resulting equations. The material properties of the beams are assumed to be graded in the thickness direction according to a simple power law distribution in terms of the volume fractions of the constituents and to be temperature-dependent. The effects of material constants, transverse shear deformation, temperature-dependent material properties, in-plane loading and boundary conditions on the nonlinear behavior of the FGM beams are discussed in details. The numerical results obtained herein show that FGM beams subjected to an in-plane thermal loading do exhibit some unique and interesting characteristics in both static and dynamic behaviors, particularly when effects of both the transverse shear deformation and the temperature-dependent material properties are simultaneously taken into consideration.

2. Basic equations

A beam made of functionally graded materials with uniform a cross-section of area A, height h and length l is considered here, as shown in Fig. 1. The Cartesian coordinate system (x, y, z), with an origin at the middle of the beam is used in this analysis. The xoy plane is taken to be the undeformed mid-plane of the beam, the x-axis coincides with the centroidal axis of the beam and z-axis is the vertical coordinate pointing upwards.

It is assumed that the material properties P (such as Young's modulus E, thermal expansion coefficient α and mass density ρ) of the beam vary through the height of beam and can be expressed as follows [24]

$$P(z) = (P_m - P_c)\left(\frac{h-2z}{2h}\right)^n + P_c \tag{1}$$

Here, the subscripts, m and c, denote the metallic and ceramic constituents, respectively, and n is the gradient index. The material properties of the form P that are temperature-dependent can be written as

$$P = P_0(P_{-1}T^{-1} + 1 + P_1T + P_2T^2 + P_3T^3) \tag{2}$$

where P_0, P_{-1}, P_1, P_2 and P_3 are the coefficients of the temperature, T(K) and are unique to each constituent. In this paper, Poisson's ratio, v is assumed to be a constant value of 0.28.

Based on the physical neutral surface concept put forward by Zhang and Zhou [27], the physical neutral surface of an FGM beam is given by $z = z_0$,

$$z_0 = \frac{\int_{-h/2}^{h/2} zE(z)\mathrm{d}z}{\int_{-h/2}^{h/2} E(z)\mathrm{d}z} \tag{3}$$

It can be seen that the physical neutral surface and the geometric middle surface are the same in a homogeneous isotropic beam.

Under the physical neutral surface concept and the first-order shear deformation nonlinear beam theory, the displacements take the following forms:

$$\begin{aligned} U_x(x,z,t) &= \bar{u}(x,t) + (z-z_0)\phi(x,t) \\ U_z(x,z,t) &= \bar{w}(x,t) \end{aligned} \tag{4}$$

where $\bar{u}$ and $\bar{w}$ are the displacements in the physical neutral surface along the coordinates x and z, respectively, while ϕ denotes the slope at $z = z_0$ of the deformed line that was straight in the undeformed beam. By using $\phi = -\frac{\partial \bar{w}}{\partial x}$ in Eq. (4), these equations are reduced to those of the classical beam theory (CBT). The strains are

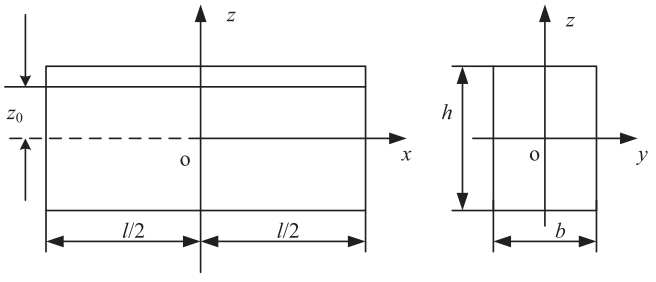

Fig. 1. Geometry and coordinates of a beam.

$$\varepsilon_x = \varepsilon_x^0 + (z-z_0)\varepsilon_x^1 = \frac{\partial \bar{u}}{\partial x} + \frac{1}{2}\left(\frac{\partial \bar{w}}{\partial x}\right)^2 + (z-z_0)\frac{\partial \phi}{\partial x}$$
$$\gamma_{xz} = \gamma_{xz}^0 = \phi + \frac{\partial \bar{w}}{\partial x} \tag{5}$$

In the above, ε_x^0 and ε_x^1 are the strain and curvature, respectively, in the physical neutral surface. γ_{xz}^0 denotes the transverse shear strain. The constitutive equations can be deduced by proper integration

$$N_x = \int_A \sigma_x dA = A_x\varepsilon_x^0 - N^T = A_x\left\{\frac{\partial \bar{u}}{\partial x} + \frac{1}{2}\left(\frac{\partial \bar{w}}{\partial x}\right)^2\right\} - N^T$$
$$M_x = \int_A \sigma_x (z-z_0) dA = D_x\varepsilon_x^1 - M^T = D_x\frac{\partial \phi}{\partial x} - M^T \tag{6}$$
$$Q_x = \int_A \tau_{xz} dA = A_{xz}\gamma_{xz}^0 = A_{xz}\left(\phi + \frac{\partial \bar{w}}{\partial x}\right)$$

where $A_x = \int_A E(z)dA$, $D_x = \int_A (z-z_0)^2 E(z)dA$, $A_{xz} = k_s\int_A \frac{E(z)}{2(1+\nu)}dA$, $(N^T, M^T) = \int_A E\alpha T\{1, (z-z_0)\}dA$, also, k_s denotes the shear correction factor, and T is the uniform rise in temperature.

It can be seen that there is no stretching–bending coupling in the constitutive equations of physical neutral surface theory.

Using Hamilton's principle, one can derive the following motion equations and boundary conditions in terms of non-dimensional variables based on the FBT

$$\frac{\partial^2 U}{\partial \xi^2} + \frac{\partial W}{\partial \xi}\frac{\partial^2 W}{\partial \xi^2} - f_3\frac{\partial^2 U}{\partial \tau^2} - f_3 f_4\left(\frac{\partial^2 \varphi}{\partial \tau^2} - \frac{\partial^3 W}{\partial \xi \partial \tau^2}\right) = 0 \tag{7a}$$

$$\frac{\partial^2 \varphi}{\partial \xi^2} - \frac{\partial^3 W}{\partial \xi^3} - f_7\frac{\partial^2 U}{\partial \tau^2} - f_2\varphi - f_6 f_8\left(\frac{\partial^2 \varphi}{\partial \tau^2} - \frac{\partial^3 W}{\partial \xi \partial \tau^2}\right) = 0 \tag{7b}$$

$$\left(1 + \frac{F_1}{f_2}\right)\frac{\partial^4 W}{\partial \xi^4} - F_1\frac{\partial^2 W}{\partial \xi^2} + 3f_5\frac{\partial}{\partial \xi}\left(F_2\frac{\partial^2 W}{\partial \xi^2}\right) + \left(f_5\frac{\partial^2 F_2}{\partial \xi^2} - \frac{f_6}{\beta^2}F_2\right)\frac{\partial W}{\partial \xi} + f_7\frac{\partial^3 U}{\partial \xi \partial \tau^2} + f_6 f_8\left(\frac{\partial^3 \varphi}{\partial \xi \partial \tau^2} - \frac{\partial^4 W}{\partial \xi^2 \partial \tau^2}\right) - \beta^2 f_5\frac{\partial^4 W}{\partial \xi^2 \partial \tau^2} + f_6\frac{\partial^2 W}{\partial \tau^2} = 0 \tag{7c}$$

$$U = 0, \quad W = 0, \quad \varphi - \frac{\partial W}{\partial \xi} = 0 \quad \text{for a clamped end} \tag{8a}$$

$$U = 0, \quad W = 0, \quad \frac{\partial \varphi}{\partial \xi} - \frac{\partial^2 W}{\partial \xi^2} - \overline{M} = 0 \quad \text{for a simply supported end} \tag{8b}$$

where

$$F_1 = f_1\left\{\frac{\partial U}{\partial \xi} + \frac{1}{2}\left(\frac{\partial W}{\partial \xi}\right)^2\right\} - N \quad \text{and}$$
$$F_2 = \frac{\partial^2 U}{\partial \tau^2} + f_4\left(\frac{\partial^2 \varphi}{\partial \tau^2} - \frac{\partial^3 W}{\partial \xi \partial \tau^2}\right).$$

The non-dimensional variables are defined as follows

$$\xi = \frac{x}{l}, \quad W = \frac{\bar{w}}{h}, \quad U = \frac{l}{h^2}\bar{u}, \quad \psi = \frac{l}{h}\phi, \quad \varphi = \psi + \frac{\partial W}{\partial \xi},$$
$$\beta = \frac{l}{h}, \quad \tau = t\Lambda^{-1/2}, \quad \overline{M} = \frac{M^T l^2}{D_x h}, \quad N = \frac{N^T l^2}{D_x}, \quad f_1 = \frac{A_x h^2}{D_x},$$
$$f_2 = \frac{A_{xz}l^2}{D_x}, \quad f_3 = \frac{I_0 l^2}{A_x \Lambda}, \quad f_4 = \frac{I_1}{I_0 h}, \quad f_5 = \frac{I_0 h^2}{A_{xz}\Lambda}, \quad f_6 = \frac{I_0 l^4}{D_x \Lambda},$$
$$f_7 = \frac{I_1 l^2 h}{D_x \Lambda}, \quad f_8 = \frac{I_2}{I_0 l^2}, \quad \text{and} \quad \Lambda = \frac{\rho_{m0} A l^4}{D_{m0}}.$$

where $(I_0, I_1, I_2) = \int_A \rho(z)\left\{1, (z-z_0), (z-z_0)^2\right\}dA$, $D_{m0} = \frac{E_{m0}bh^3}{12}$.

3. Nonlinear static behavior

The governing equations of the nonlinear static problem of an FGM beam under an in-plane thermal loading can be obtained from Eq. (7) by neglecting the inertial terms. The results are as follows

$$\frac{d^2 U_s}{d\xi^2} + \frac{dW_s}{d\xi}\frac{d^2 W_s}{d\xi^2} = 0$$
$$\frac{d^2 \varphi_s}{d\xi^2} - \frac{d^3 W_s}{d\xi^3} - f_2\varphi_s = 0$$
$$\left\{1 + \frac{1}{f_2}\left[f_1\left\{\frac{dU_s}{d\xi} + \frac{1}{2}\left(\frac{dW_s}{d\xi}\right)^2\right\} - N\right]\right\}\frac{d^4 W_s}{d\xi^4} - \left[f_1\left\{\frac{dU_s}{d\xi} + \frac{1}{2}\left(\frac{dW_s}{d\xi}\right)^2\right\} - N\right]\frac{d^2 W_s}{d\xi^2} = 0 \tag{9}$$

$$U_s = 0, \quad W_s = 0, \quad \varphi_s - \frac{dW_s}{d\xi} = 0 \quad \text{for a clamped end} \tag{10a}$$

$$U_s = 0, \quad W_s = 0, \quad \frac{d\varphi_s}{d\xi} - \frac{d^2 W_s}{d\xi^2} - \overline{M} = 0 \quad \text{for a simply supported end} \tag{10b}$$

where U_s, ϕ_s and W_s are the displacements of the nonlinear static equilibrium configuration of an FGM beam.

To understand the nonlinear static behavior of an FGM beam subjected to an in-plane thermal loading, studies have been carried out on stainless steel (SUS304)–silicon nitride (Si_3N_4) FGM beams. The temperature coefficients corresponding to Si_3N_4 and SUS304 are listed in Table 1. It is assumed that the temperature in the stress free state is 300 K. Fig. 2 shows the variations of Young's modulus along the thickness of the beam for various values of n, as calculated from Eqs. (1) and (2). It is evident that an increase in gradient index, n, results in an increase in Young's modulus and the bending rigidity.

We employ the shooting method, as earlier used in [24], to obtain the nonlinear static configuration and vibration modes and the corresponding natural frequencies as will be presented in the next section.

The typical thermal post-buckling paths of clamped FGM beams are shown in Fig. 3. Fig. 3a represents the results of shear deformable beams for various values of gradient index, n, and Fig. 3b for various values of the slenderness ratio, l/h. Fig. 3c depicts the results for classical beams for different values of gradient index, n. FBT results for FGM beams for $n = 1.0$ are compared with the CBT results in Fig. 3d. Also shown in Fig. 3a and d is the variation of dimensionless midspan deflection with dimensionless thermal loading, λ ($\lambda = 12\beta^2\alpha_{m0}\Delta T$, where ΔT is the temperature rise from the stress free state) for pure metal and ceramic beams. The solid and dashed lines denote the results for beams with temperature independent material properties (referred to as TID) and temperature-dependent material properties (referred to as TD), respectively. As expected, in Fig. 3a, it can be seen that the shape of post-buckling load–deflection curves for FGM beams appear quite similar to that for pure material beams; further, the dimensionless midspan deflection of the FGM beams with material properties between those of ceramic and metal is intermediate to the deflection of ceramic and metal beams. This can be attributed to the fact that Young's modulus of ceramic is the highest and that of metal the lowest. A similar discussion holds good for the classical results shown in Fig. 3c. It can be seen from Fig. 3b that the post-buckling deflection decreases with an increase in slenderness ratio because

Table 1
Temperature dependent coefficients for Si_3N_4 and SUS304.

Material	Properties	P_0	P_{-1}	P_1	P_2	P_3
Si_3N_4	E [Pa]	348.43e+9	0.0	−3.070e−4	2.160e−7	−8.946e−11
	α [K^{-1}]	5.8723e−6	0.0	9.095e−4	0.0	0.0
	ρ [kg/m^3]	2370.0	0.0	0.0	0.0	0.0
SUS304	E [Pa]	201.04e+9	0.0	3.079e−4	−6.534e−7	0.0
	α [K^{-1}]	12.330e−6	0.0	8.086e−4	0.0	0.0
	ρ [kg/m^3]	8166.0	0.0	0.0	0.0	0.0

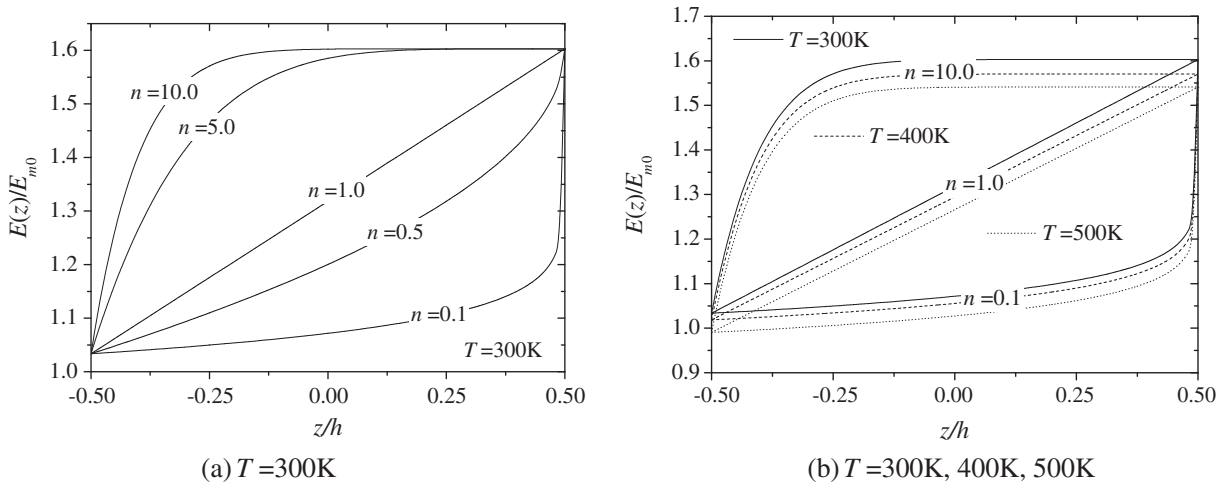

Fig. 2. Variation of Young's modulus through thickness of the FGM beam for different values of n.

this means a reduction in the influence of transverse shear deformation. As expected, compared to the shear deformable beams, the classical beams have a higher critical thermal buckling load and lower post-buckling deflection, particularly when temperature-dependent material properties are taken into consideration as shown in Fig. 3d. From Fig. 3, it can also be observed that the critical thermal buckling load of the FGM beams has reduced when the temperature-dependent material properties are considered; in contrast with this, the temperature-dependent material properties result in an increase in the deflection of FGM beams.

Fig. 4 demonstrates the variation of dimensionless critical thermal buckling load, λ_{cr}, with gradient index, n, based on the FBT for various values of slenderness ratio, l/h. Also shown in Fig. 4 are the classical results. It is clear that there is a sharp increase in the dimensionless buckling temperature at the early stage of n; the critical buckling temperature increases slowly with an increase in gradient index, n, as it approaches the homogenous ceramic composition. This trend is to be expected because Young's modulus of ceramic is higher than that of metal. It is also seen from Fig. 4 that as the value of the slenderness ratio, l/h, increases, the critical buckling temperature increases up to the classical results. Such a trend is observed because the effect of transverse shear deformation is ignored in the classical beam theory.

Fig. 5 shows the variation of dimensionless midspan deflection $W_s(0)$ with thermal load for a simply supported FGM beam based on the FBT. Also shown in Fig. 5d are the classical results. It is seen from Fig. 5 that simply supported FGM beams under an in-plane thermal load exhibit quite different behavior from the thermal post-buckling of clamped FGM beams, as shown in Fig. 3. Transverse displacements occur no matter how small the in-plane loads; therefore, there is no bifurcation buckling in this case, which further verify the conclusion made by several investigators [18–21]. From Fig. 5, it is also seen that there are two different solution branches of the load–deflection curve for simply supported FGM beams under an in-plane thermal load, which appear quite similar to the behavior corresponding to imperfect beams, as elaborated in [28]. Furthermore, depending on the load level, the beams may have three different values of deflection corresponding to a given load, that is, three deformed configurations may exist for a simply supported FGM beam for a given load, as shown in Fig. 6, but the minimum configuration for which the magnitude of deflection is the smallest over all three configurations is unstable, as pointed out by Looss and Joseph [28].

The variation of deflection with thermal load for a simply supported FGM beam with and without temperature-dependent properties is shown in Fig. 7 for different values of slenderness ratio, l/h, and in Fig. 8 for different value of gradient index, n. The results in Fig. 7a and Fig. 8a (resp., Fig. 7b and Fig. 8b) are presented for a beam with TID (resp., TD). It can be observed from Fig. 7 when the temperature-dependent material properties are taken into consideration that the transverse shear deformation strongly influences the load–deflection curves. In contrast, if the material properties are independent of temperature, the transverse shear deformation does not much influence the load–deflection curves. In Fig. 8, it is also seen that the temperature-dependent material properties significantly affect the deflection of a simply supported FGM beam.

The FBT results for simply supported FGM beams under an in-plane thermal loading are compared with corresponding results based on the CBT in Fig. 9. The results in Fig. 9a are presented for a beam with TID and the results in Fig. 9b for a beam with TD. In Fig. 9, it is seen that the FBT results for the beams are almost identical to the classical results when the material properties are assumed to be constant with respect to the temperature. In contrast, if the material properties are dependent on the temperature, the transverse shear deformation strongly influences the load–deflection curves, which trend is similar to that observed in Fig. 7.

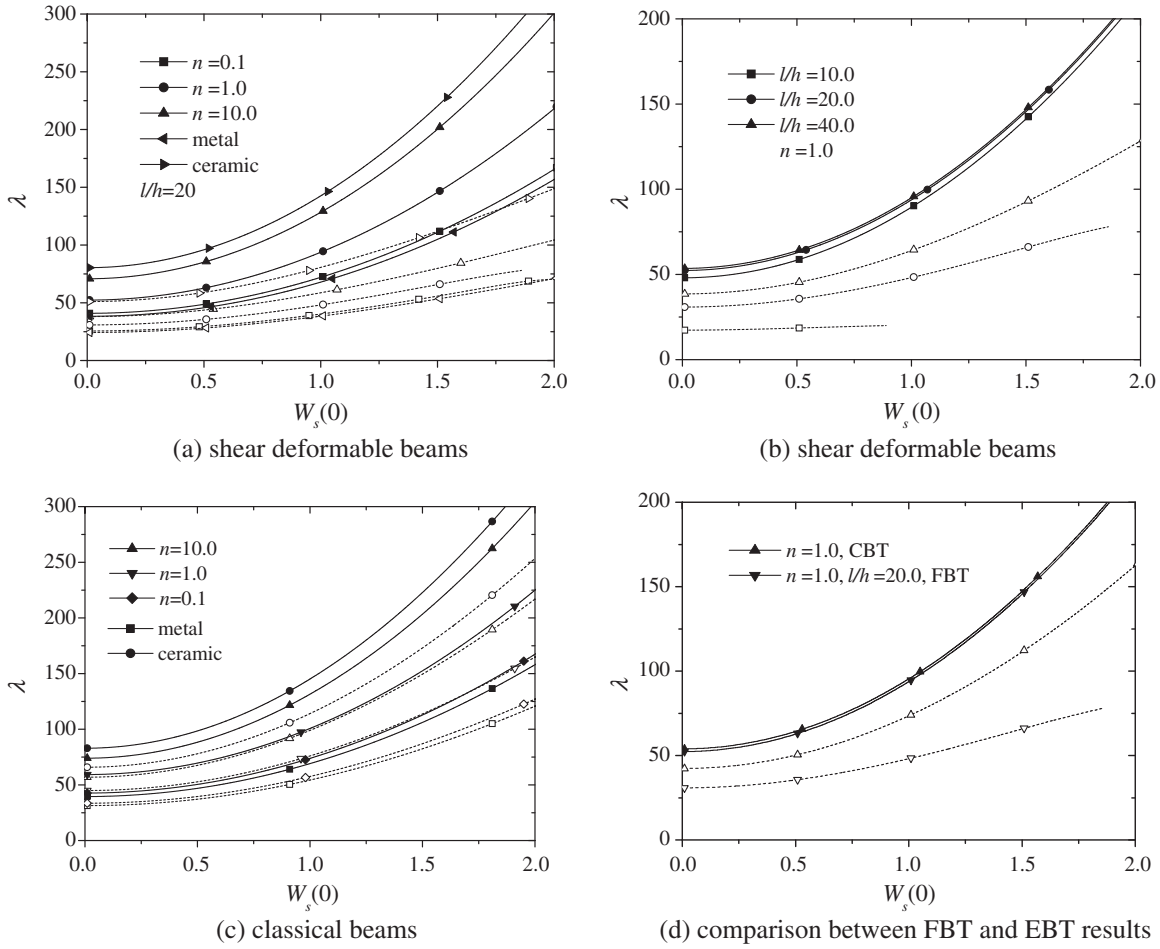

Fig. 3. Post-buckling paths of clamped FGM beams.

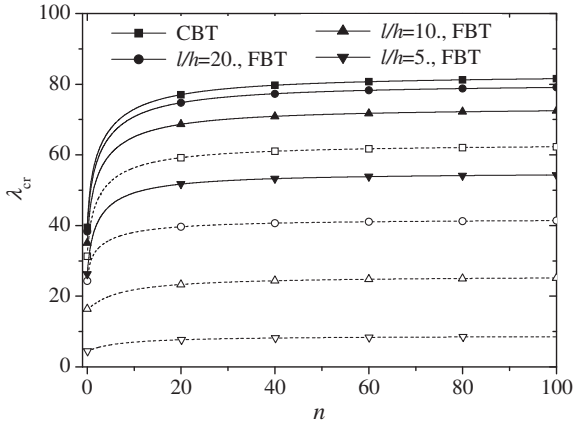

Fig. 4. Variation of critical thermal buckling load with gradient index.

4. Dynamic response

Now, we turn our attention to the dynamic response of FGM beams under an in-plane thermal loading.

In this investigation, we focus on steady-state vibrations corresponding to infinitesimal deformations that are superimposed upon the static nonlinear deformed configuration of an FGM beam. We seek solutions of Eqs. (7) and (8) of the following form [29,30]

$$\begin{aligned} U(\xi,\tau) &= U_s(\xi) + U_d(\xi,\tau) \\ \varphi(\xi,\tau) &= \varphi_s(\xi) + \varphi_d(\xi,\tau) \\ W(\xi,\tau) &= W_s(\xi) + W_d(\xi,\tau) \end{aligned} \tag{11}$$

where $U_d(\xi,\tau)$, $\phi_d(\xi,\tau)$ and $W_d(\xi,\tau)$ are the dynamic responses near the nonlinear static equilibrium configuration for the FGM beam.

Substituting Eq. (11) into Eqs. (7) and (8), using Eqs. (9) and (10) and neglecting the nonlinear terms $U_d(\xi,\tau)$, $\phi_d(\xi,\tau)$ and $W_d(\xi,\tau)$, we obtain the following equations for determining U_d, ϕ_d and W_d:

$$\frac{\partial^2 U_d}{\partial\xi^2} + \frac{\mathrm{d}^2 W_s}{\mathrm{d}\xi^2}\frac{\partial W_d}{\partial\xi} + \frac{\mathrm{d}W_s}{\mathrm{d}\xi}\frac{\partial^2 W_d}{\partial\xi^2} - f_3\frac{\partial^2 U_d}{\partial\tau^2} - f_3 f_4\left(\frac{\partial^2\varphi_d}{\partial\tau^2} - \frac{\partial^3 W_d}{\partial\xi\partial\tau^2}\right) = 0 \tag{12a}$$

$$\frac{\partial^2\varphi_d}{\partial\xi^2} - \frac{\partial^3 W_d}{\partial\xi^3} - f_2\varphi_d - f_7\frac{\partial^2 U_d}{\partial\tau^2} - f_6 f_8\left(\frac{\partial^2\varphi_d}{\partial\tau^2} - \frac{\partial^3 W_d}{\partial\xi\partial\tau^2}\right) = 0 \tag{12b}$$

$$\begin{aligned} &\left\{1 + \frac{F_{1s}}{f_2}\right\}\frac{\partial^4 W_d}{\partial\xi^4} - F_{1s}\frac{\partial^2 W_d}{\partial\xi^2} + \frac{f_1}{f_2}\left(\frac{\partial U_d}{\partial\xi} + \frac{\mathrm{d}W_s}{\mathrm{d}\xi}\frac{\partial W_d}{\partial\xi}\right)\frac{\mathrm{d}^4 W_s}{\mathrm{d}\xi^4} \\ &\quad + 3f_5\left(F_{2d}\frac{\mathrm{d}^3 W_s}{\mathrm{d}\xi^3} + \frac{\partial F_{2d}}{\partial\xi}\frac{\mathrm{d}^2 W_s}{\mathrm{d}\xi^2}\right) \\ &\quad - f_1\left(\frac{\partial U_d}{\partial\xi} + \frac{\mathrm{d}W_s}{\mathrm{d}\xi}\frac{\partial W_d}{\partial\xi}\right)\frac{\mathrm{d}^2 W_s}{\mathrm{d}\xi^2} \\ &\quad + f_5\frac{\partial^2 F_{2d}}{\partial\xi^2}\frac{\mathrm{d}W_s}{\mathrm{d}\xi} - \frac{f_6}{\beta^2}F_{2d}\frac{\mathrm{d}W_s}{\mathrm{d}\xi} - \beta^2 f_5\frac{\partial^4 W_d}{\partial\xi^2\partial\tau^2} \\ &\quad + f_6\frac{\partial^2 W_d}{\partial\tau^2} + f_7\frac{\partial^3 U_d}{\partial\xi\partial\tau^2} + f_6 f_8\left(\frac{\partial^3\varphi_d}{\partial\xi\partial\tau^2} - \frac{\partial^4 W_d}{\partial\xi^2\partial\tau^2}\right) = 0 \end{aligned} \tag{12c}$$

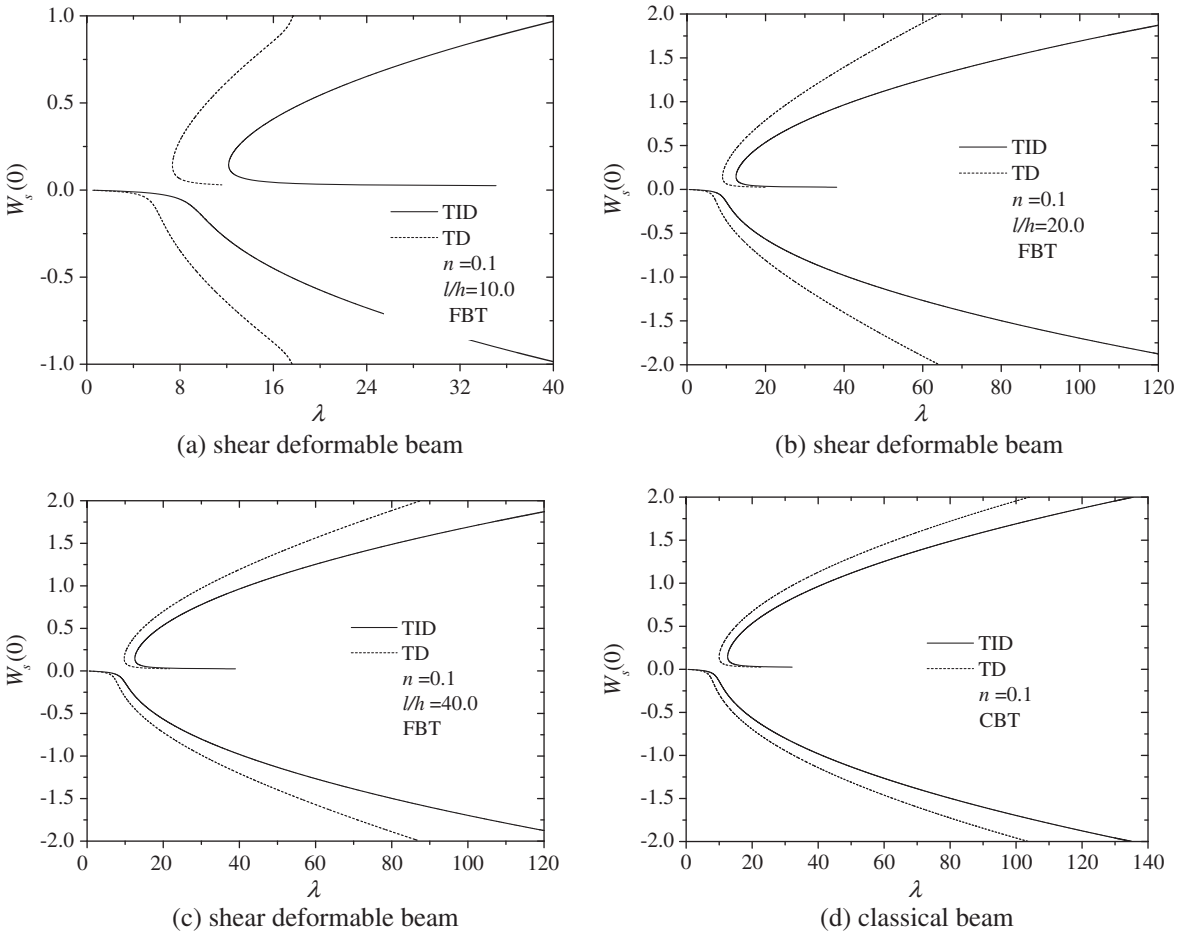

Fig. 5. Load–deflection curves of simply supported FGM beams.

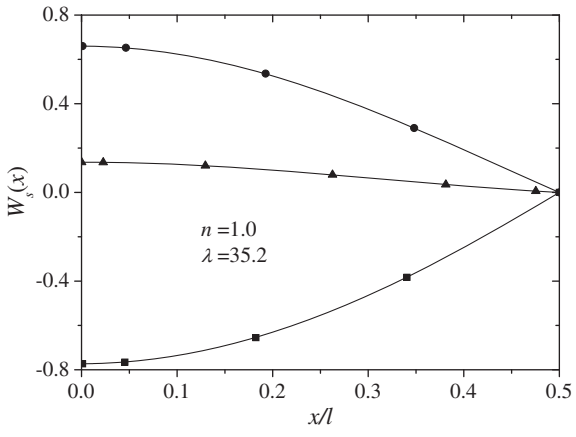

Fig. 6. Bending configurations of simply supported FGM beams based on the CBT.

$$U_d = 0, \quad W_d = 0, \quad \varphi_d - \frac{\partial W_d}{\partial \xi} = 0 \quad \text{for a clamped end} \tag{13a}$$

$$U_d = 0, \quad W_d = 0, \quad \frac{\partial \varphi_d}{\partial \xi} - \frac{\partial^2 W_d}{\partial \xi^2} = 0 \quad \text{for a simply supported end} \tag{13b}$$

where

$$F_{1s} = f_1 \left\{ \frac{\mathrm{d}U_s}{\mathrm{d}\xi} + \frac{1}{2}\left(\frac{\mathrm{d}W_s}{\mathrm{d}\xi}\right)^2 \right\} - N \quad \text{and}$$

$$F_{2d} = \frac{\partial^2 U_d}{\partial \tau^2} + f_4 \left(\frac{\partial^2 \varphi_d}{\partial \tau^2} - \frac{\partial^3 W_d}{\partial \xi \partial \tau^2} \right).$$

It should be noted that the method employed here is not based on the superposition of solutions to the static and dynamic problems as is commonly used in linear problems. Here, it is a process of decomposition rather than superposition [31]. On substitution of Eq. (11) into Eqs. (7) and (8), the static parts of the resulting equations are the same as the static beam equations based on the FBT (that is, Eqs. (9) and (10)). Upon subtracting the static equations from the aforementioned resulting equations and by considering small amplitude vibration in the vicinity of nonlinear static equilibrium, the dynamic equations are generated. The solution process involves solving Eqs. (9) and (10) to generate the static solution, which in turn, is substituted in Eqs. (12) and (13) to derive the dynamic solution.

If the beam is not buckled or bended, that is, $\phi_s(\xi) = W_s(\xi) = 0$, then Eqs. (12) and (13) govern the linear vibrations of a pre-buckled beam.

We assume that Eqs. (12) and (13) have a solution of the form [29,30]

$$\{U_d(\xi,\tau), \varphi_d(\xi,\tau), W_d(\xi,\tau)\} = \{u(\xi), \bar{\varphi}(\xi), w(\xi)\} e^{i\omega\tau} \tag{14}$$

where $\omega = \bar{\omega}\sqrt{\Lambda}$, $\bar{\omega}$ is the natural frequency of the beam. The substitution of Eq. (14) into Eqs. (12) and (13) yield the following ordinary differential equations for the amplitudes, $u(\xi)$, $\bar{\varphi}(\xi)$ and $w(\xi)$.

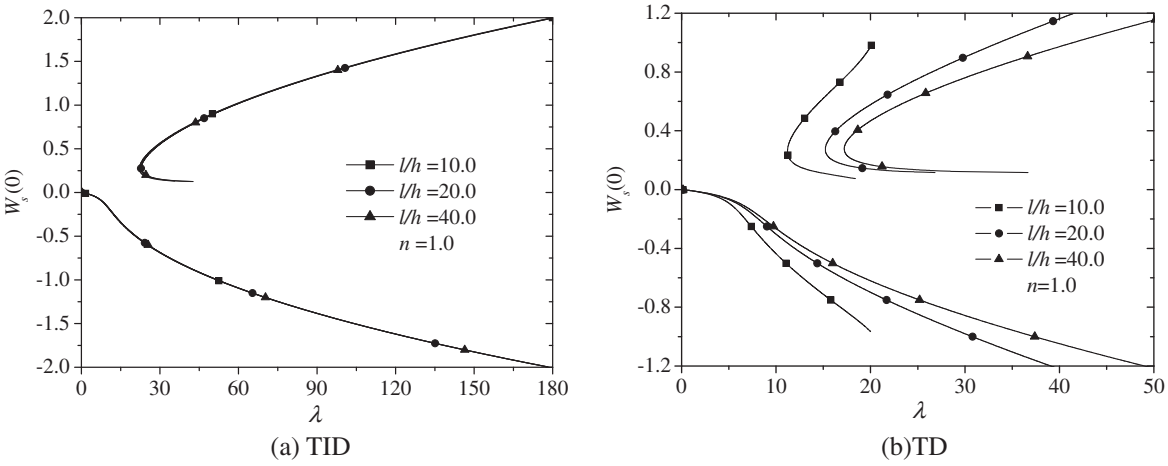

Fig. 7. Variation of midspan deflection for a simply supported FGM beam with thermal load for different values of the slenderness ratio.

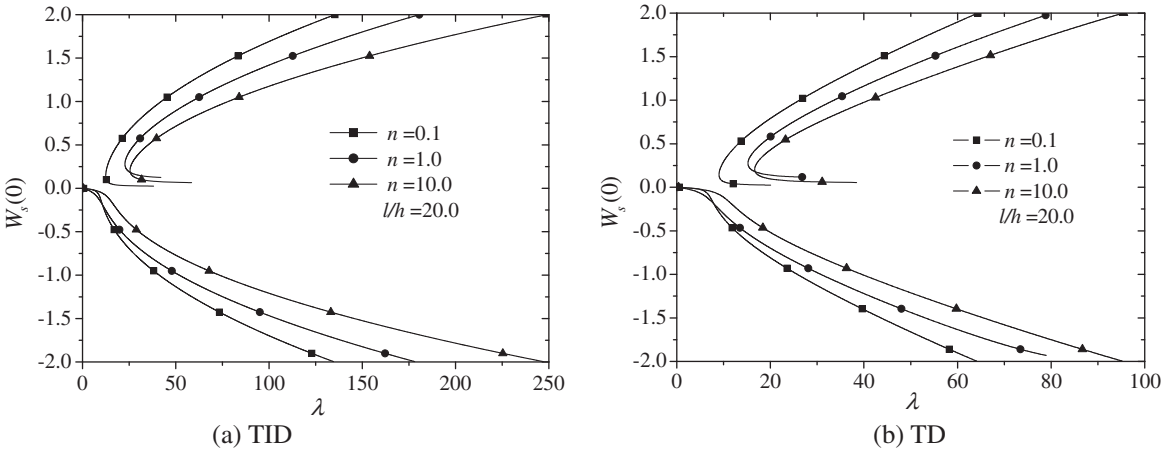

Fig. 8. Variation of midspan deflection for a simply supported FGM beam with thermal load for different values of gradient index.

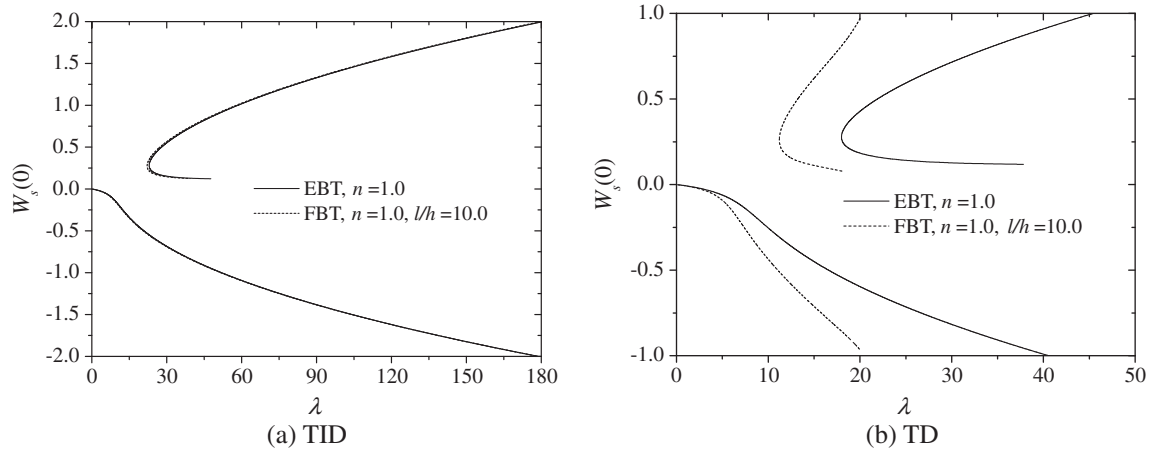

Fig. 9. FBT and CBT results on bending for a simply supported FGM beam.

$$\frac{d^2u}{d\xi^2}+\frac{d^2W_s}{d\xi^2}\frac{dw}{d\xi}+\frac{dW_s}{d\xi}\frac{d^2w}{d\xi^2}+f_3\omega^2u+f_3f_4\omega^2\left(\bar{\varphi}-\frac{dw}{d\xi}\right)=0 \tag{15a}$$

$$\frac{d^2\bar{\varphi}}{d\xi^2}-\frac{d^3w}{d\xi^3}-f_2\bar{\varphi}+f_7\omega^2u+f_6f_8\omega^2\left(\bar{\varphi}-\frac{dw}{d\xi}\right)=0 \tag{15b}$$

$$\left(1+\frac{F_{1s}}{f_2}\right)\frac{d^4w}{d\xi^4}-F_{1s}\frac{d^2w}{d\xi^2}+\frac{f_1}{f_2}\left(\frac{du}{d\xi}+\frac{dW_s}{d\xi}\frac{dw}{d\xi}\right)\frac{d^4W_s}{d\xi^4}$$
$$-f_1\left(\frac{du}{d\xi}+\frac{dW_s}{d\xi}\frac{dw}{d\xi}\right)\frac{d^2W_s}{d\xi^2}-3f_5\omega^2\frac{d}{d\xi}\left(F_3\frac{d^2W_s}{d\xi^2}\right)$$
$$-f_5\omega^2\frac{d^2F_3}{d\xi^2}\frac{dW_s}{d\xi}+\frac{f_6}{\beta^2}\omega^2F_3\frac{dW_s}{d\xi}-f_7\omega^2\frac{du}{d\xi} \quad (15c)$$
$$-f_6f_8\omega^2\left(\frac{d\bar{\varphi}}{d\xi}-\frac{d^2w}{d\xi^2}\right)+\beta^2f_5\omega^2\frac{d^2w}{d\xi^2}-f_6\omega^2w=0$$

$$u=0,\quad w=0,\quad \bar{\varphi}-\frac{dw}{d\xi}=0 \quad \text{for a clamped end} \quad (16a)$$

$$u=0,\quad w=0,\quad \frac{d\bar{\varphi}}{d\xi}-\frac{d^2w}{d\xi^2}=0 \quad \text{for a simply supported end} \quad (16b)$$

where $F_3=u+\left(\bar{\varphi}-\frac{dw}{d\xi}\right)$.

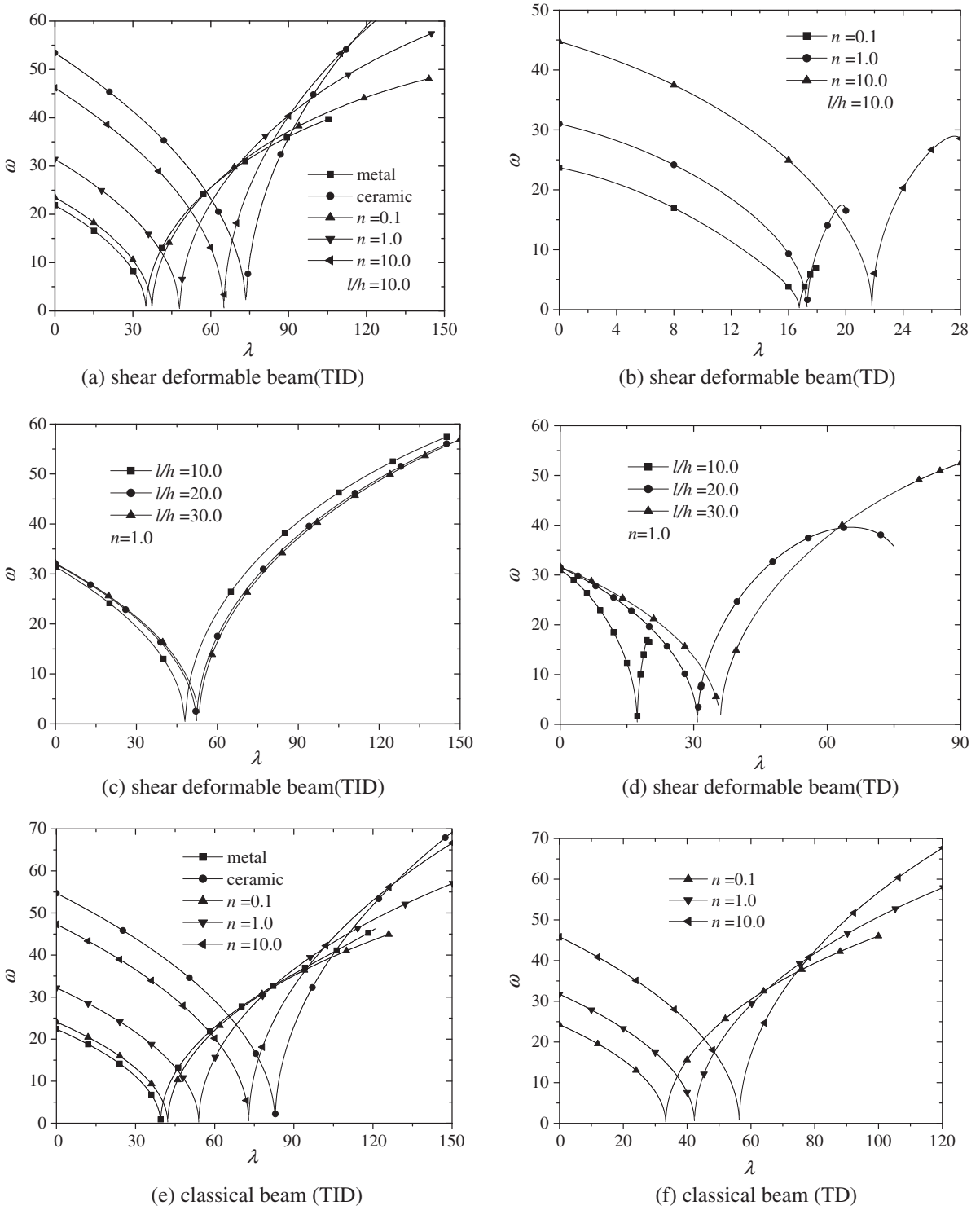

(a) shear deformable beam(TID) (b) shear deformable beam(TD)

(c) shear deformable beam(TID) (d) shear deformable beam(TD)

(e) classical beam (TID) (f) classical beam (TD)

Fig. 10. Variation of natural frequency of vibration near the buckled configuration with thermal load for a clamped FGM beam.

We note that Eqs. (15) and (16) are the same as those of free vibration for FGM beams with initial deformations of U_s, φ_s and W_s. However, here the initial deformations are unknown, and are to be determined by solving the coupled nonlinear Eqs. (9) and (10).

By simultaneously solving the boundary-value problems, Eqs. (9) and (10) and Eqs. (15) and (16), we get frequencies and the corresponding mode shapes of a thermally deformed FGM beam with either a simply supported or a clamped boundary condition.

Fig. 10 presents the variation of the natural frequency for clamped FGM beams in both the pre-buckling and post-buckling domains. The results in Fig. 10a–d are presented for shear deformable beams and the results in Fig. 10e and f for classical beams. The results in Fig. 10a, c and e are presented for beams with TID and the results in Fig. 10b, d and f are for beams with TD. Also shown in Fig. 10a and e are the results for pure metal and ceramic beams. In the pre-buckling domain, the natural frequency decreases as the thermal load increases until it reaches zero at the onset of

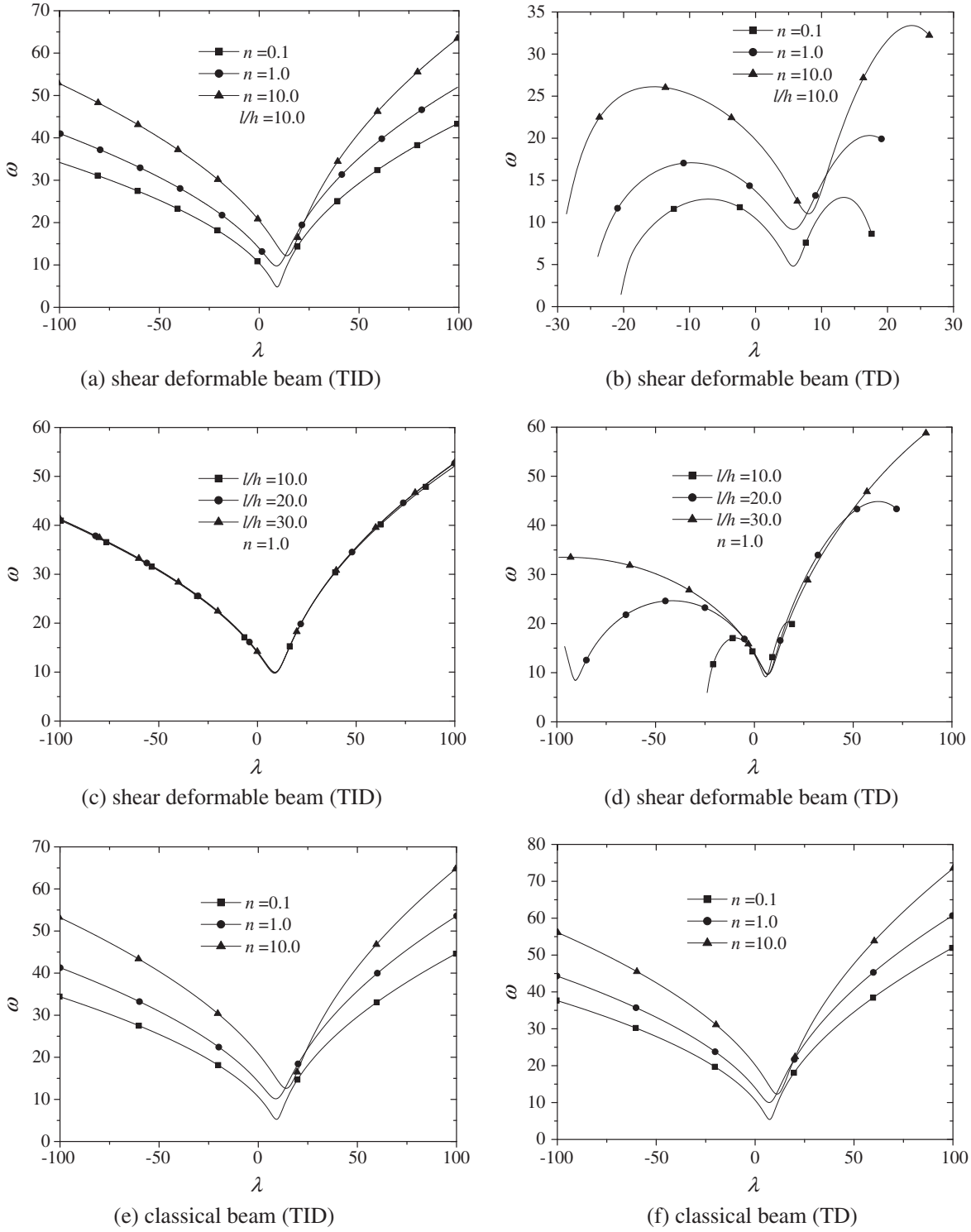

Fig. 11. Variation of natural frequency of vibration near the nonlinear static bended configuration with thermal load for a simply supported FGM beam.

buckling as expected, regardless of whether or not the material properties are dependent on the temperature. This decrease in frequency with thermal load is attributed to the fact that the thermally induced compressive stress weakens the beam stiffness. In the post-buckling domain, the fundamental natural frequency increases monotonously with an increase in thermal load when temperature-dependent material properties are not taken into consideration, as shown in Fig. 10a, c and e; this is quite similar to the trend for homogenous or composite beams observed in [29,30]. Thereby, this increase in frequency with thermal load implies that a buckled beam can support additional loads without failure. Furthermore, we see that the characteristic curves are continuous but not differentiable at $\lambda = \lambda_{cr}$. The results plotted in Fig. 3 suggest that this is a bifurcation point from which the beam goes into the secondary equilibrium path from the initial straight equilibrium state. The pre-buckling and post-buckling equilibrium

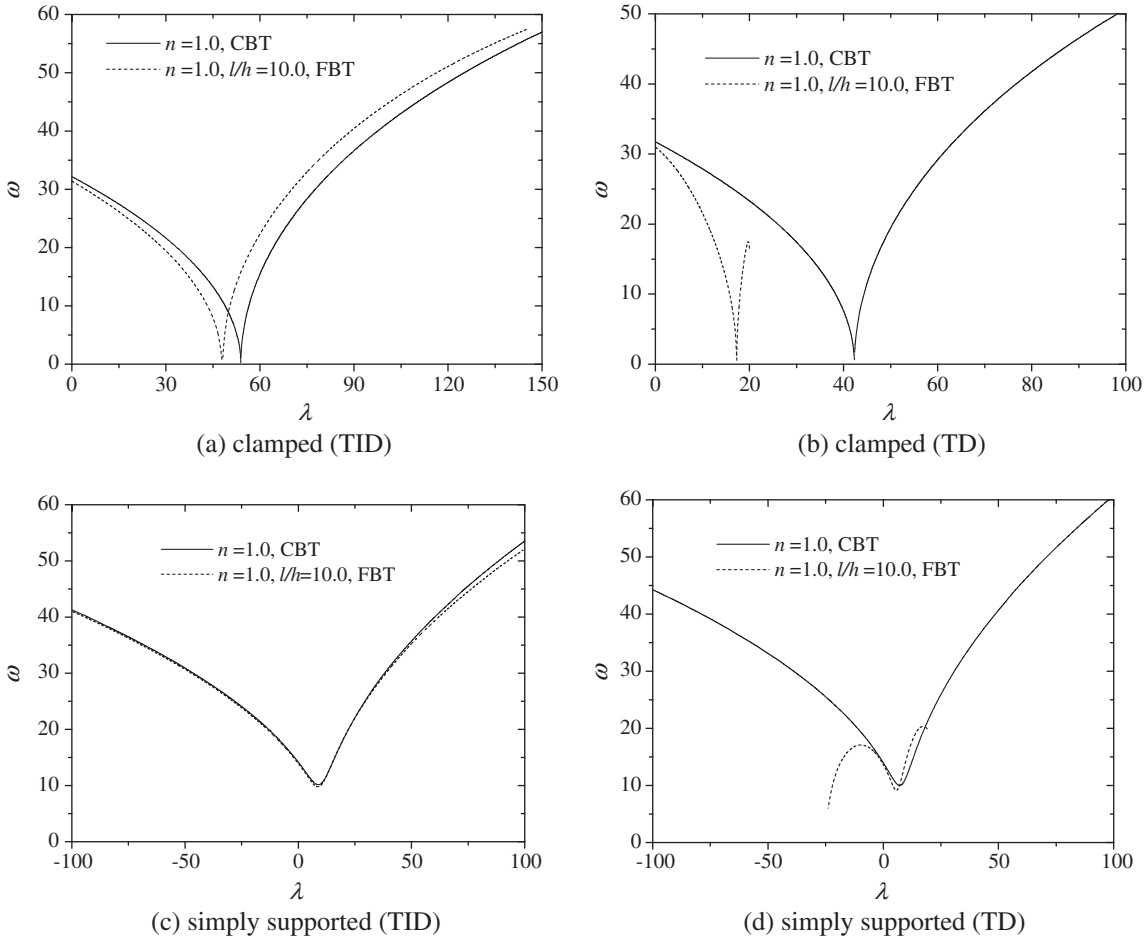

Fig. 12. Comparison of load–frequency curves between a shear deformable beam and a classical beam.

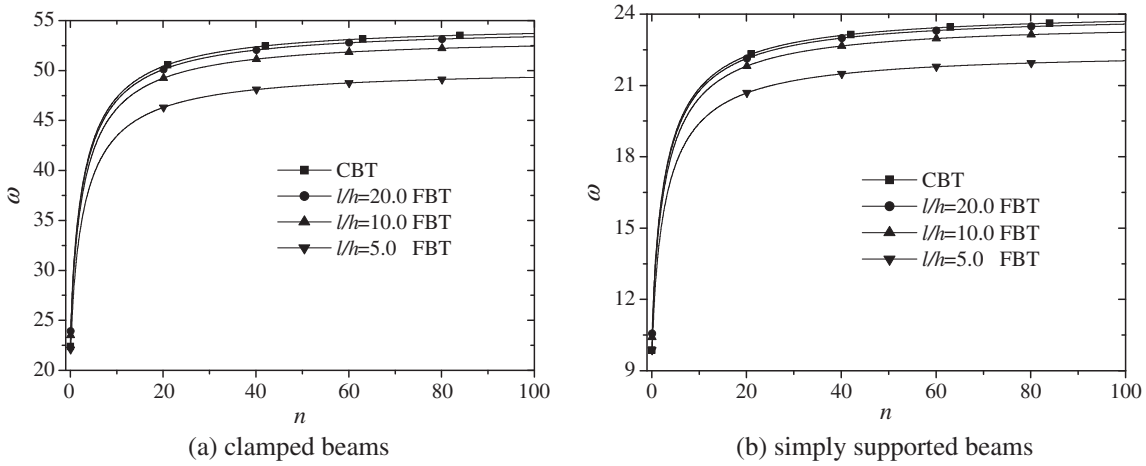

Fig. 13. Variation of dimensionless fundamental frequency with gradient index.

configurations of the beam are totally different. A similar discussion holds good for classical results that account for the variation in material properties with respect to the temperature and are shown in Fig. 10f. However, if the transverse shear deformation and temperature-dependent material properties are simultaneously taken into consideration, the natural frequency increases initially with an increase in the thermal load and reaches a peak value and thereafter reduces rapidly, particularly when the value of the slenderness ratio, l/h, is small, as shown in Fig. 10b and d. This is quite different from the behavior of FGM beams with TID, as shown in Fig. 10a, c and e and for homogenous or composite beams, as observed in [29,30]. In Fig. 10c, for a given value of the thermal load, when the slenderness ratio, l/h, is larger, the natural frequency is higher in the pre-buckling domain and lower in the post-buckling domain.

The variation of natural frequency of vibration in the vicinity of the nonlinear static bended configuration for a simply supported FGM beams with thermal load is shown in Fig. 11. In Fig. 11a–d, the results for shear deformable beams are displayed and the results for classical beams are shown in Fig. 11e and f. The results in Fig. 11a, c and e are presented for a beam with TID and the results in Fig. 11b, d and f are for a beam with TD. We note that dynamic behavior of simply supported FGM beams is quite different from that of clamped FGM beams, as observed in Fig. 10. It is seen from Fig. 11a, c, e and f that the natural frequency decreases initially with an increase in the thermal load and reaches its minimum value; thereafter, it increases. However, if the effects of the transverse shear deformation and temperature-dependent material properties are simultaneously taken into consideration, the natural frequency increases up to a certain value, then decreases and again starts increasing up to a peak value; thereafter, it reduces rapidly, particularly when the value of the slenderness ratio, l/h, is small, as shown in Fig. 11b and d. This is quite different from the trend for FGM beams with TID, as shown in Fig. 11a and c. It also can be observed from Fig. 11c and d when the temperature-dependent material properties are taken into consideration that the transverse shear deformation strongly influences the load–frequency curves. In contrast, if the material properties are independent of the temperature, the transverse shear deformation does not much influence the load–frequency curves. As a result, the transverse shear deformation and temperature-dependent material properties play an important role in the dynamic behavior of the FGM beam.

Fig. 12 shows a comparison of frequency between a shear deformable beam with $n = 1.0$ and $l/h = 10.0$ and a classical beam with $n = 1.0$. Fig. 12a and b denote the results for a clamped beam and a simply supported beam, respectively. Fig. 12a and c are the results for a beam with TID. The results for a beam with TD are shown in Fig. 12b and d. For a clamped beam, the transverse shear deformation significantly affects the natural frequency, particularly when the temperature-dependent material properties are taken into account. For a simply supported beam, the transverse shear deformation does not much affect the natural frequency when the temperature-dependent material properties are independent of the temperature. In contrast, if the material properties are dependent on the temperature, the transverse shear deformation strongly influences the frequency, as shown in Fig. 12d.

Fig. 13 shows the variations of dimensionless fundamental frequency with gradient index for clamped and simply supported FGM beams, respectively, based on the FBT. Also shown in Fig. 13 are the classical results. It is clearly seen from these figures that the dimensionless frequencies increase with an increase in gradient index, n, as discussed in Fig. 4 for a critical buckling thermal load.

Fig. 14 shows the effect of slenderness ratio on dimensionless fundamental frequency of an FGM beam when $\lambda = 0$. The results in Fig. 14a and b are for beams with clamped and simply supported edges, respectively. As expected, an increase in the slenderness ratio results in an increase in the dimensionless fundamental frequency. This is because as the value of l/h increases, the influence

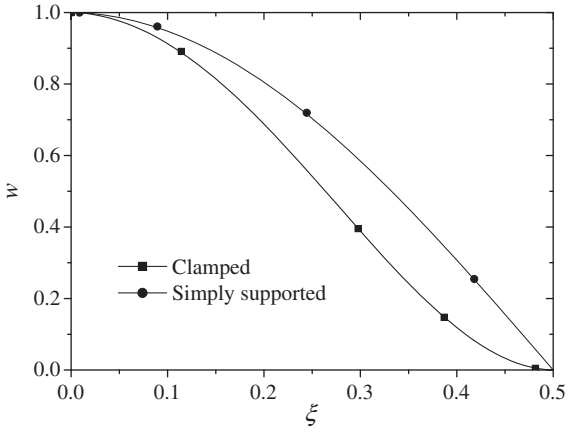

Fig. 15. Mode shapes of FGM beams based on the FBT.

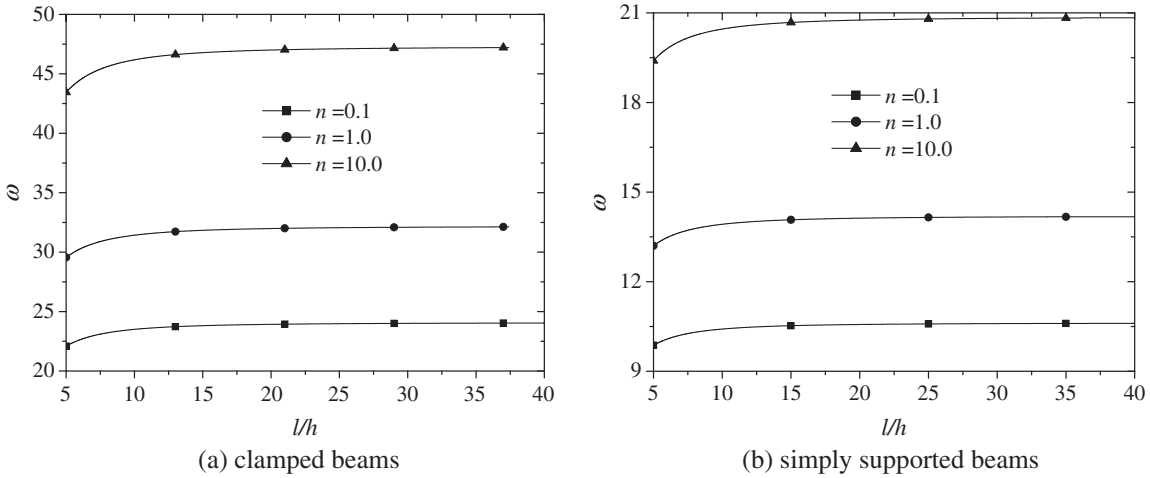

Fig. 14. Variation of dimensionless fundamental frequency with slenderness.

of the transverse shear deformation becomes smaller and the beam has larger transverse shear stiffness.

Fig. 15 shows the mode shapes of FGM beams with clamped and simply supported edges. The results obtained herein indicate that the mode shapes of the FGM beams are independent of gradient index, n.

5. Conclusions

The following conclusions are arrived from present study.

Under an in-plane thermal loading, clamped FGM beams exhibit typical thermal post-buckling behaviors. All the beams with intermediate properties undergo corresponding intermediate values of the midspan deflection. The transverse deflection of a simply supported FGM beam subjected to an in-plane thermal load is initiated, regardless of the magnitude of the loading. As a consequence, the bifurcation buckling does not occur for simply supported FGM beams. The load–deflection curve for simply supported beams has two different branches and three deformed configurations may exist for a given thermal load.

An increase in the gradient index, n, results in an increase in the dimensionless critical buckling temperature for a clamped FGM beam and a decrease in deflection of such an FGM beam. The dimensionless natural frequency for FGM beams increases as the gradient index, n, increases when the material properties are independent of the temperature.

Temperature-dependent material properties result in an increase in the deflection, a reduction in the thermal buckling strength of an FGM beam, and a decrease in the dimensionless natural frequency for FGM beams.

An increase in the slenderness ratio, l/h, results in a reduction in the influence of the transverse shear deformation. As a consequence, the dimensionless critical buckling temperature and the natural frequency of classical beams are higher than those of shear deformable beams. In contrast with this, the deflection of classical beams is lower than that of shear deformable beams.

Various factors such as material constants, the transverse shear deformation, temperature-dependent material properties, in-plane loading, slenderness ratio and boundary conditions play important roles in the static response and dynamic behavior of FGM beams.

Acknowledgements

This work was supported by the Korea Science & Engineering Foundation through the NRL Program (Grant R0A-2007-000-10157-0) and WCU (World Class University) program through the National Research Foundation of Korea funded by the Ministry of Education, Science and Technology (R32-20087).

References

[1] Librescu L, Oh SY, Song O. Thin-walled beams made of functionally graded materials and operating in a high temperature environment: vibration and stability. J Therm Stresses 2005;28:649–712.
[2] Birman V, Byrd LW. Modeling and analysis of functionally graded materials and structures. Appl Mech Rev 2007;60:195–216.
[3] Bhangale RK, Ganesan N. Thermoelastic vibration and buckling analysis of functionally graded sandwich beam with constrained viscoelastic core. J Sound Vib 2006;295:294–316.
[4] Ying J, Lu CF, Chen WQ. Two-dimensional elasticity solutions for functionally graded beams resting on elastic foundations. Compos Struct 2008;84:209–19.
[5] Chakraborty A, Gopalakrishnan S, Reddy JN. A new beam finite element for the analysis of functionally graded materials. Int J Mech Sci 2003;45(3):519–39.
[6] Aydogdu M, Taskin V. Free vibration analysis of functionally graded beams with simply supported edges. Mater Des 2007;28(5):1651–6.
[7] Kapuria S, Bhattacharyya M, Kumar AN. Bending and free vibration response of layered functionally graded beams: a theoretical model and its experimental validation. Compos Struct 2008;82(3):390–402.
[8] Yang J, Chen Y. Free vibration and buckling analyses of functionally graded beams with edge cracks. Compos Struct 2008;83(1):48–60.
[9] Li XF. A unified approach for analyzing static and dynamic behaviors of functionally graded Timoshenko and Euler–Bernoulli beams. J Sound Vib 2008;318(4–5):1210–29.
[10] Yang J, Chen Y, Xiang Y, Jia XL. Free and forced vibration of cracked inhomogeneous beams under an axial force and a moving load. J Sound Vib 2008;312(1–2):166–81.
[11] Xiang HJ, Yang J. Free and forced vibration of a laminated FGM Timoshenko beam of variable thickness under heat conduction. J Compos: Part B 2008;39:292–303.
[12] Lu CF, Chen WQ. Free vibration of orthotropic functionally graded beams with various end conditions. Struct Eng Mech 2005;13:1430–7.
[13] Zhong Z, Yu T. Analytical solution of a cantilever functionally graded beam. Compos Sci Technol 2007;67:481–8.
[14] Sina SA, Navazi HM, Haddadpour H. An analytical method for free vibration analysis of functionally graded beams. Mater Des 2009;30:741–7.
[15] Pradhan SC, Murmu T. Thermo-mechanical vibration of FGM sandwich beam under variable elastic foundations using differential quadrature method. J Sound Vib 2009;321:342–62.
[16] Simsek M, Kocatürk T. Free and forced vibration of a functionally graded beam subjected to a concentrated moving harmonic load. Compos Struct 2009;90:465–73.
[17] Li Y, Shi ZF. Free vibration of a functionally graded piezoelectric beam via state-space based differential quadrature. Compos Struct 2009;87:257–64.
[18] Leissa AW. Conditions for laminated plates to remain flat under inplane loading. Compos struct 1986;6(4):262–70.
[19] Leissa AW. A review of laminated composite plate buckling. Appl Mech Rev 1987;40(5):575–91.
[20] Qatu MS, Leissa AW. Buckling or transverse deflections of unsymmetrically laminated plates subjected to in-plane loads. AIAA J 1993;31(1):189–94.
[21] Shen HS. Bending, buckling and vibration of functionally graded plates and shells. Adv Mech 2004;34(1):53–60 [In Chinese].
[22] Aydogdu M. Conditions for functionally graded plates to remain flat under in-plane loads by classical plate theory. Compos Struct 2008;82:155–7.
[23] Shen HS. Nonlinear bending response of functionally graded plates subjected to transverse loads and in thermal environments. Int J Mech Sci 2002;44:561–84.
[24] Ma LS, Wang TJ. Nonlinear bending and post-buckling of a functionally graded circular plate under mechanical and thermal loadings. Int J Solids struct 2003;40(13–14):3311–30.
[25] Ma LS, Wang TJ. Axisymmetric post-buckling of a functionally graded circular plate subjected to uniformly distributed radial compression. Mater Sci Forum 2003;423–424:719–24.
[26] Morimoto T, Tanigawa Y, Kawamura R. Thermal buckling of functionally graded rectangular plates subjected to partial heating. Int J Mech Sci 2006;48:926–37.
[27] Zhang DG, Zhou YH. A theoretical analysis of FGM thin plates based on physical neutral surface. Comput Mater Sci 2008;44:716–20.
[28] Looss G, Joseph DD. Elementary stability and bifurcation theory. 2nd ed. New York: Springer; 1990.
[29] Emam SA, Nayfeh AH. Postbuckling and free vibrations of composite beams. Compos Struct 2009;88:636–42.
[30] Li SR, Batra RC, Ma LS. Vibration of thermally post-buckled orthotropic circular plates. J Therm Stresses 2007;30:43–57.
[31] Zhou YH, Zheng XJ, Harik IE. Free-vibration analysis of compressed clamped circular plates. J Eng Mech ASCE 1995;121(12):1372–6.